Supporting information for High-throughput transport-of-intensity quantitative phase imaging with aberration correction

Linpeng Lu,[†,‡,¶] Shun Zhou,[†,‡,¶] Yefeng Shu,[†,‡,¶] Yanbo Jin,[†,‡,¶] Jiasong Sun,[†,‡,¶] Ran Ye,[*,†,§] Maciej Trusiak,[*,‖] Peng Gao,[*,⊥] and Chao Zuo[*,†,‡,¶]

†*Smart Computational Imaging Laboratory (SCILab), School of Electronic and Optical Engineering, Nanjing University of Science and Technology, Nanjing, Jiangsu Province 210094, China*

‡*Smart Computational Imaging Research Institute (SCIRI) of Nanjing University of Science and Technology, Nanjing, Jiangsu Province 210019, China*

¶*Jiangsu Key Laboratory of Spectral Imaging & Intelligent Sense, Nanjing, Jiangsu Province 210094, China*

§*School of Computer and Electronic Information, Nanjing Normal University, Nanjing 210023, China*

‖*Institute of Micromechanics and Photonics, Warsaw University of Technology, 8 Sw. A. Boboli St., Warsaw 02-525, Poland*

⊥*School of Physics, Xidian University, Xi'an, China*

E-mail: ran.ye@njnu.edu.cn; maciej.trusiak@pw.edu.pl; peng.gao@xidian.edu.cn; zuochao@njust.edu.cn

ABSTRACT

This document provides supporting information for "High-throughput transport-of-intensity quantitative phase imaging with aberration correction". We discuss in detail the algorithm steps, simulation results for optimal illumination configuration design of the proposed TI-AC method, comparison between AO-QPI and TI-AC and spatially variant aberrations correction of TI-AC.

CONTENTS

1. The specific algorithm of TI-AC

The specific steps of the proposed TI-AC algorithm are as follows:

Step 1: data acquisition. Obtain a stack of defocus intensity of N z-axis measurements $I^n_{mea}(\mathbf{r})$, where $n = 1, 2, ..., N$ $(N = 12)$, and $\mathbf{r}$ is a two-dimensional coordinate in real space, $\mathbf{r} = (x, y)$. The intensity measurements are captured by a defocus distance step-size of 1 μm under annular NA-matched illumination. When the value of n equals to 1, it means that the image is in-focus intensity.

Step 2: initialization. In the upsampled process, we assume that the actual pixel size of the sensor is reduced to one-third of the actual situation to guarantee the Nyquist sampling criterion and those low-resolution images are captured when pixel binning is enabled (3×3 pixels are combined into one pixel). Thus, we upsample the in-focus intensity image $I^1_{mea}(\mathbf{r})$ by a down-sampling factor of $K = 3$. Then use the upsampled image $I_{up}(\mathbf{r})$ and zero-valued phase to initialize the complex amplitude of the sample, $O(\mathbf{r}) = \sqrt{I_{up}(\mathbf{r})}e^{j\phi(\mathbf{r})}$, where $\phi(\mathbf{r})$ is the phase of the high resolution object function distribution $O(\mathbf{r})$. The pupil function $\hat{P}(\mathbf{u})$ ($\mathbf{u}$ is the spatial frequency coordinate corresponding to $\mathbf{r}$) can be initialized as a circular distribution with zero phase aberration, whose cutoff frequency depending on the objective NA and illumination wavelength λ, i.e., NA/λ.

Step 3: coherent mode decomposition and numerical propagation. Based on the assumed complex amplitude of object $O(\mathbf{r})$ and pupil function $\hat{P}(\mathbf{u})$ from Step 2 under the annular NA-matched illumination distribution ($NA_i = NA_o$), we can obtain a stack of intensity images corresponding to each LED individually illuminated

$$I^n_i(\mathbf{r}) = |\mathscr{F}^{-1}\{\mathscr{P}[\hat{P}(\mathbf{u})\hat{O}(\mathbf{u} - \mathbf{u}_i)]\}|^2 \tag{S1}$$

where i means the diversity angle of LED illumination $[i = 1, 2, ..., I$ $(I = 12)]$, $\mathscr{F}^{-1}$ is two dimensional inverse Fourier transform, $|\cdot|^2$ represents the intensity for complex amplitude, $\hat{O}(\mathbf{u})$ is the Fourier transform of high-resolution object function $O(\mathbf{r})$, i.e., $\hat{O}(\mathbf{u}) = \mathscr{F}\{O(\mathbf{r})\}$,

and $\mathbf{u}_i$ indicates the spatial frequency vector of the i-th LED illumination. Besides, $\mathscr{P}$ is numerical propagation process and can be expressed as $e^{jkz_{step}n(\sqrt{1-\lambda^2|\mathbf{u}|^2})}$, where k is wave number, z_{step} is the step-size of defocus distance along the optical axis.

Step 4: intensity constraint. Perform incoherent superposition of the intensities $I_i^n(\mathbf{r})$ at the same defocus distance (under the same n) but different illumination angles (under the diversity i) to calculate the partially coherent illumination intensity image $I_{cal}^n(\mathbf{r})$, and then decompose the acquired measurements $I_{mea}^n(\mathbf{r})$ into intensity components $I_{dec,i}^n(\mathbf{r})$ of the complex amplitude $U_i^n(\mathbf{u})$

$$I_{dec,i}^n(\mathbf{r}) = \frac{|\mathscr{F}^{-1}\{\hat{U}_i^n(\mathbf{u})\}|^2}{\sum_{i=1}^{I=12} I_i^n(\mathbf{r})} I_{mea}^n(\mathbf{r}) \tag{S2}$$

According to the pixel binning model, $I_{cal}^n(\mathbf{r}) = \sum_{i=1}^{I=12} I_i^n(\mathbf{r})$ here is the version after down-sampling by $K = 3$. And the decomposition principle is based on the fact that the measured intensities $I_{mea}^n(\mathbf{r})$ satisfy the principle of incoherent superposition, i.e., the image acquired when all 12 LEDs are simultaneously illuminated is equal to the sum of the images acquired when each LED is individually illuminated. Then, the 3 times upsampling version of the decomposed intensity images $I_{dec,i}^n(\mathbf{r})$ are used as the intensity constraint condition to update the normalized complex amplitude $U_i^n(\mathbf{r})$. The update formula is derived as

$$U_i(\mathbf{r}) = \mathscr{P}^{-1}\{\sqrt{I_{dec,i}^n(\mathbf{r})}\frac{U_i^n(\mathbf{r})}{|U_i^n(\mathbf{r})|}\} \tag{S3}$$

where $U_i(\mathbf{r})$ is the inverse Fourier transform of the product of updated $\hat{O}(\mathbf{u})$ and $\hat{P}(\mathbf{u})$, $\mathscr{P}^{-1}$ indicates the back-propagation process in $-z_{step}$ case.

Step 5: phase recovery and aberration correction. Synthesize these propagated complex amplitude stacks $U_i(\mathbf{r})$ in the Fourier domain and perform global updates on the target's complex amplitude $O(\mathbf{r})$ based on difference map[1,2] by converting Eq. S1 into an

optimization problem, and the corresponding vectorized objective function ε is as follows:

$$\varepsilon = \sum_i \left\| \sqrt{\mathbf{I}_i} - \left| \mathbf{F}^{-1}\mathbf{P}_i\mathbf{O} \right| \right\|^2 \equiv \sum_i \left\| \sqrt{\mathbf{I}_i} - |\mathbf{g}_i| \right\|^2 \tag{S4}$$

where $\|\cdot\|$ is the Euclidean norm, $\mathbf{F}$ is the matrix representation of the discrete Fourier transform and $\mathbf{g}_i = \mathbf{F}^{-1}\mathbf{P}_i\mathbf{O}$. The matrix $\mathbf{P}_i$ is determined by $\hat{P}(\mathbf{u})$, the matrix $\mathbf{I}_i$ corresponds to the measured intensity images, and the matrix $\mathbf{O}$ is determined by $\hat{O}(\mathbf{u})$. The error metric given by Eq. S4 is also called real-space error, quantifying how closely the current estimated value fits the input data. Then, we apply the schemes of synthetic aperture and multiplexing to difference map,[1,2] which has the ability to update the entire objective function in one iteration as an iterative global algorithm. In order to analyze the difference map DM more intuitively, the following description is based on non-convex set projection theory, which is formed by the difference of a pair of basic projections $\prod_1$ and $\prod_2$ and defined as

$$DM = 1 + \beta(\prod_1 \circ f_2 - \prod_2 \circ f_1) \tag{S5}$$

where β is a non-zero real parameter, $\circ$ represents composite mapping, $\prod_1$ expresses the object domain constraint set (convex), and $\prod_2$ is the Fourier domain constraint set (non-convex). $(\prod_1 \circ f_2 - \prod_2 \circ f_1)$ is the difference of the two projection operators, each composed with a map f_i: $E^N \to E^N$. The recovery process is to enforce the known object $\prod_1$ and Fourier domain $\prod_2$ constraints through the framework of alternating projection as Eq. S5. For effectively decoupling the system, it is necessary to take turns applying the two equations several iterations (which is beneficial for finding the minimum value), thereby achieving phase recovery and pixel super-resolution.

To correct phase aberrations, we use the embedded pupil function recovery (EPRY) algorithm[3] and Zernike polynomial constraints. After updating the pupil function using EPRY to provide physical prior constraints for aberrations, Zernike polynomial constraints of n-order are used as the basis functions to fit the retrieved aberrations, improving convergence

efficiency. Due to the coupling effect between phase and aberrations under partially coherent illumination, it is necessary to first perform separate phase recovery (with a small number of iterations) and then simultaneously reconstruct the phase and aberrations to improve the quality of aberration correction. Since TI-AC only uses brightfield intensity images as input data, the formula for coherent ePIE case has been updated as shown in Eq. S6 [4,5]

$$\hat{P}_i(\mathbf{u}) = \hat{P}(\mathbf{u}) + \alpha \frac{\hat{O}(\mathbf{u})^*}{|\hat{O}(\mathbf{u})|^2} [\hat{U}_i^{(j)}(\mathbf{u}) - \hat{U}_i^{(j-1)}(\mathbf{u})] \tag{S6}$$

and then the global updating is implemented by using difference map. [1] Here, $\hat{U}_i^{(j)}(\mathbf{u})$ and $\hat{U}_i^{(j-1)}(\mathbf{u})$ are the Fourier spectrum with and without the intensity constraint respectively, j is the current iteration, and α is the updating step size. By repeating Steps 3 to 5 until convergence or reach a certain number of iterations, the high-resolution complex amplitude U with aberration correction can be recovered.

2. Minimum data redundancy criteria for TI-AC

In phase retrieval, successful recovery relies on sufficient data redundancy as it is a typical ill-posed inverse problem. Considering the additional reconstruction of the system pupil, it can be inferred that the requirement for data redundancy becomes even more demanding. To achieve aberration correction with high imaging efficiency, we discussed deeper into the minimum data redundancy criteria necessary for successful aberration correction in TI-AC. Using the previously mentioned NA-matched illumination configuration, we simulate the recovery of pupil aberration using varying numbers of raw images, as illustrated in Fig. S1.

Figures S1(a1) and S1(a2) are the input specimen phase and input aberration of the simulation. In Fig. S1(b), we show the reconstructed aberrations with different number of raw images. Besides, we provide the convergence curves of pupil function error in Fig. S1(c). It can be observed that when the number of input data is less than 12 images, the convergence speed is slow and the reconstructed aberration exhibits significant low-frequency

artifacts, which reduces the accuracy of aberration correction. Our findings indicate that by incorporating the uniform transmission assumption and the Zernike polynomial constraint into the aberration recovery process, the TI-AC method can achieve successful phase retrieval using 12 images. Furthermore, increasing the number of raw images does not significantly improve the quality of the reconstructed phase. Consequently, by utilizing the annular NA-matched illumination configuration with the Zernike polynomial constraint, only 12 images could realize the aberration correction for our proposed TI-AC method.

3. Comparison between AO-QPI and TI-AC

To verify the advantage of TI-AC using annular illumination in acquiring high-SNR intensity, we compared TI-AC with the AO-QPI method under a 12-piece LED setup and the same exposure time of 15 ms per frame. AO-QPI acquires a total of 6 in-focus intensity images as raw data through point-by-point illumination, whose brightfield in-focus intensity is shown in Fig. S2(a1). TI-AC collects 12 through-focus intensity images under annular illumination, and its in-focus intensity is shown in Fig. S2(b1). The comparison between Figs. S2(a1) to (b1) shows that the dynamic range of brightfield intensity in AO-QPI differs by several orders of magnitude from TI-AC, and the SNR between corresponding intensity images is quite different as well. The intensity images acquired by TI-AC have better SNR with full advantage of the detector dynamic range. It is verified that the proposed TI-AC method has higher dynamic range (better SNR) of input data due to multiplexed illumination. To assess the tolerance of the TI-AC method for imperfect matched illumination, we conducted a simulation using the TI-AC retrieved phase of HeLa cells in the main text of Fig. 4. Specifically, the outer diameter of the annular illumination was varied from the optimal 1 (NA-matched illumination) to 0.95. Phase recovery was then performed using both AO-QPI and the proposed TI-AC method, yielding the reconstructed phase results depicted in Figs. S2(a2) and S2(b2), respectively. The results indicate that under suboptimal illu-

mination conditions, AO-QPI tends to underestimate the low-frequency components of the phase. Conversely, the TI-AC method is capable of accurately quantifying the low-frequency phase components. This suggests that the TI-AC method reduces the stringent illumination matched requirements typically associated with FPM for the recovery of low-frequency sample information. In the TI-AC method, each point light source belongs to simultaneous illumination rather than sequential illumination, and a stable global unique solution can be obtained based on the global update method of difference map. Therefore, even though perfect matching is not feasible in practical experimental setups, the TI-AC method can enhance the tolerance for illumination mismatch.

4. Spatially variant aberrations correction of TI-AC

During the development of our algorithm for image reconstruction, we have incorporated several strategies to mitigate and correct for these aberrations. For example, considering the spatially varying aberrations present in a large FOV, TI-AC digitally segments the entire FOV into sub-regions to reconstruct the corresponding aberrations separately. As shown in Fig. S3, it presents a typical example of aberration reconstruction from the center to the edge of the FOV, illustrating the spatially varying aberrations and emphasizing the importance of sub-regional aberration correction.

References

(1) V. Elser, "Phase retrieval by iterated projections," J. Opt. Soc. Am. A **20**, 40–55 (2003).

(2) L. Lu, J. Li, Y. Shu, J. Sun, J. Zhou, E. Y. Lam, Q. Chen, and C. Zuo, "Hybrid brightfield and darkfield transport of intensity approach for high-throughput quantitative phase microscopy," Advanced Photonics **4**, 056002 (2022).

(3) X. Ou, G. Zheng, and C. Yang, "Embedded pupil function recovery for fourier ptychographic microscopy," Optics Express **22**, 4960–4972 (2014).

(4) Y. Shu, J. Sun, J. Lyu, Y. Fan, N. Zhou, R. Ye, G. Zheng, Q. Chen, and C. Zuo, "Adaptive optical quantitative phase imaging based on annular illumination fourier ptychographic microscopy," PhotoniX **3**, 1–15 (2022).

(5) M. Andrew, R. John, "An improved ptychographical phase retrieval algorithm for diffractive imaging," Ultramicroscopy **109**, 1256–1262 (2009).

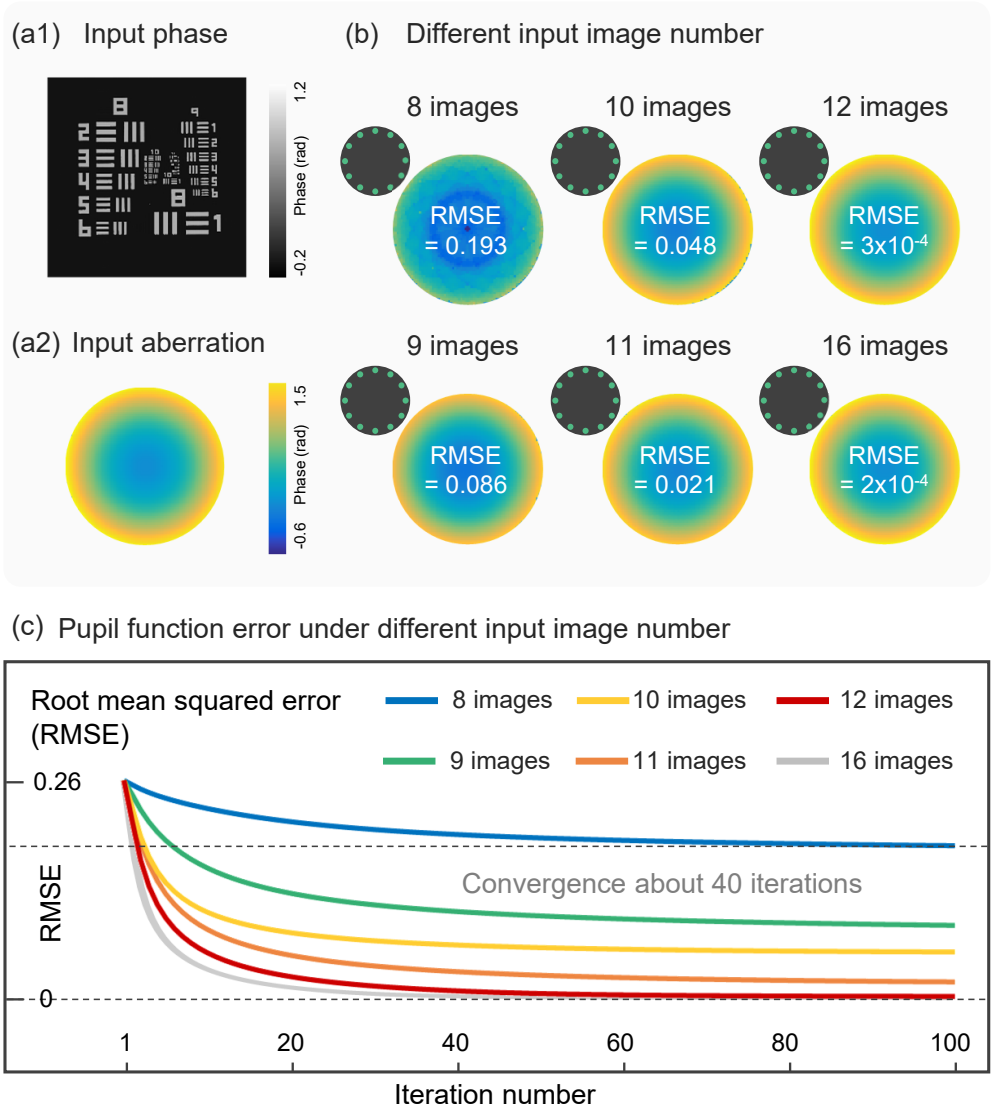

Figure S1: The comparison of the reconstructed results under the annular matched illumination with different number of images. (a1) (a2) Input specimen phase and input aberration of the simulation. (b) The reconstructed aberrations using the algorithm of TI-AC. (c) Comparison of pupil function error (RMSE) in different amount of data under the same illumination.

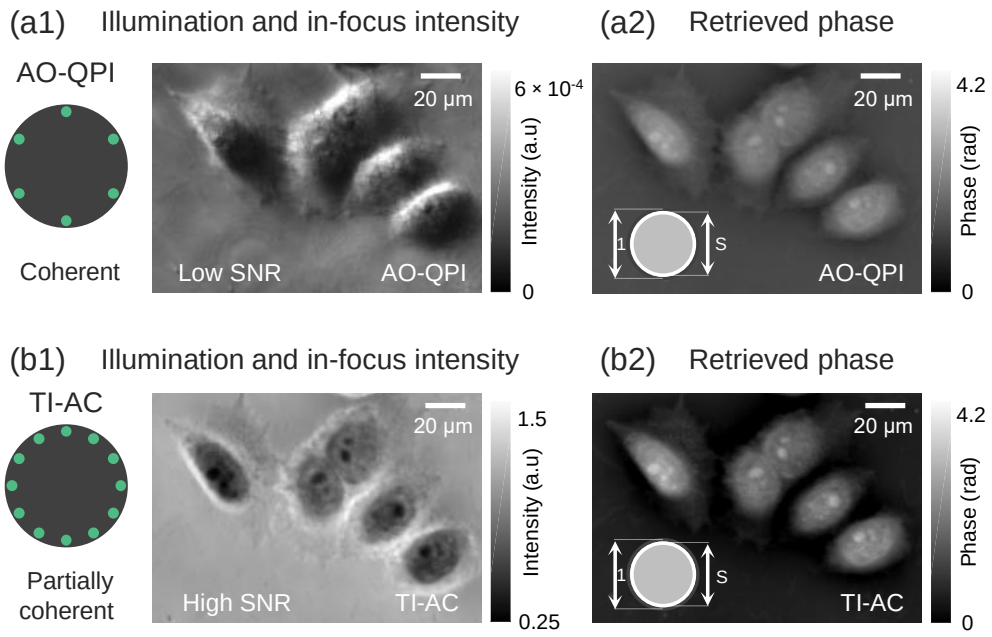

Figure S2: Comparison between the AO-QPI method and TI-AC method. (a1) The in-focus brightfield in-focus intensity of AO-QPI. (b1) The in-focus brightfield in-focus intensity of TI-AC. (a2) Phase retrieved by AO-QPI under $S = 0.95$. (b2) Phase retrieved by TI-AC under $S = 0.95$.

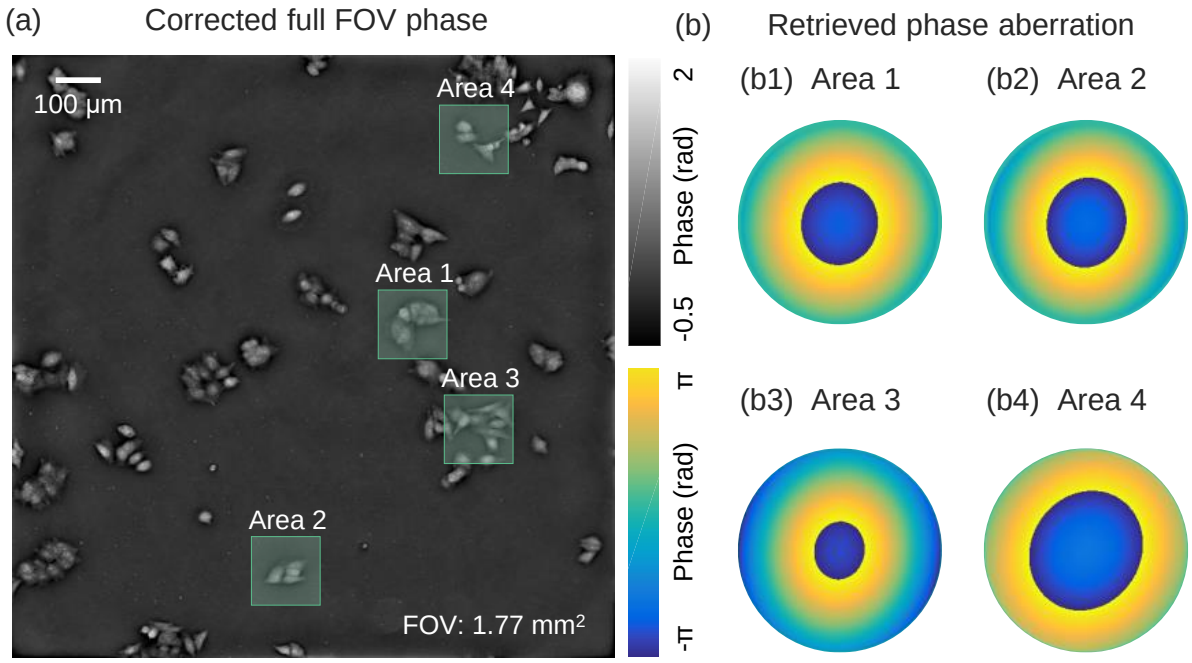

Figure S3: Retrieved phase aberrations corresponding to Area 1 to Area 4 shown in Fig. 4 (a1). (a) Corrected full FOV phase by TI-AC. (b) Retrieved phase aberration in Area 1 to Area 4.